

Study of Interstellar Molecular Clouds using Formaldehyde Absorption toward Extragalactic Radio Sources

E. D. Araya¹, N. Dieter-Conklin², W. M. Goss³, N. Andreev¹

ABSTRACT

We present new Very Large Array 6 cm H₂CO observations toward four extragalactic radio continuum sources (B0212+735, 3C 111, NRAO 150, BL Lac) to explore the structure of foreground Galactic clouds as revealed by absorption variability. This project adds a new epoch in the monitoring observations of the sources reported by Marscher and collaborators in the mid 1990's. Our new observations confirm the monotonic increase in H₂CO absorption strength toward NRAO 150. We do not detect significant variability of our 2009 spectra with respect to the 1994 spectra of 3C111, B0212+735 and BL Lac; however we find significant variability of the 3C111 2009 spectrum with respect to archive observations conducted in 1991 and 1992. Our analysis supports that changes in absorption lines could be caused by chemical and/or geometrical gradients in the foreground clouds, and not necessarily by small scale (~ 10 AU) high density molecular clumps within the clouds.

Subject headings: ISM: molecules – radio lines

1. Introduction

The 6 cm line of formaldehyde (H₂CO) is a powerful probe to study molecular gas in the Milky Way and in other galaxies (e.g., Mangum et al. 2008; Dickel et al. 2001). Soon after its discovery (Snyder et al. 1969), the H₂CO 6 cm transition was detected in absorption toward radio continuum sources as well as against the Cosmic Microwave Background (e.g.,

¹Physics Department, Western Illinois University, 1 University Circle, Macomb, IL 61455, USA

²Emeritus, Radio Astronomy Laboratory, University of California, Berkeley, USA

³National Radio Astronomy Observatory, P.O. Box 0, Socorro, NM 87801, USA

Palmer et al. 1969; Dieter 1973). Now, more than 40 years of observations have shown that the 6 cm H_2CO line can trace large ($> 5\text{pc}$) molecular clouds (e.g., Araya et al. 2007). Such large structures are not homogeneous, for example, Dieter-Conklin (2010) concluded that molecular clouds traced by H_2CO absorption show different velocity dispersion when observed at effective resolutions greater or smaller than $\sim 0.5\text{pc}$, which gives direct evidence for sub-parsec structure traced by H_2CO .

Even smaller size-scales can be probed by H_2CO observations of absorption against compact extragalactic radio sources. In particular, Marscher et al. (1993) and Moore & Marscher (1995) used the VLA to monitor 6 cm H_2CO absorption toward four extragalactic radio sources during a period of 3.4 years, and found evidence for H_2CO line variability toward three continuum sources (3C 111, NRAO 150, BL Lac; they found no significant change in the B0212+735 line profile based on observations conducted less than 2 years apart). As recognized by Marscher et al. (1993) and Moore & Marscher (1995), the variability most likely traces changes in our line of sight that occurs because we move with respect to the distant source and intervening cloud, i.e., the combined effect of Earth’s revolution around the Sun and the cloud’s internal kinematics and proper motion (see Dieter-Conklin 2009, for a discussion of this “searchlight effect”). Marscher et al. (1993) estimated that the change in line of sight through the clouds enables probing physical scales of the order of 4 AU per year, i.e., $\sim 14\text{AU}$ for sources with 3.4 years monitoring data.

The use of 6 cm H_2CO absorption as probe for substructure (as revealed by spectral line variability) has clear advantages, in particular, the supercooling effect of the lowest K-doublet transition due to H_2 - H_2CO collisions (Townes & Cheung 1969; Thaddeus 1972; Garrison et al. 1975; Troscompt et al. 2009a) enhances the optical depth against continuum sources. Also, the separation between the main group of five hyperfine lines (centered near the $F = 2-2$ component) and the $F = 1-0$ component is approximately 18.2 kHz (equivalent to 1.13km s^{-1} ; see Tucker et al. 1970) and therefore the $F = 1-0$ line does not significantly overlaps with the main hyperfine components in diffuse/translucent regions and dark clouds (which have linewidths of $\lesssim 1\text{km s}^{-1}$; see for example Araya et al. 2006). Thus, if variability is detected in the main absorption feature, variability of the hyperfine component is also expected, which is a useful test to assess whether artifacts are present in the data.

The monitoring of the H_2CO line profiles started by Marscher and collaborators did not continue. In this paper we report new observations of the sources observed by Moore & Marscher (1995) to investigate longer term variability in the absorption profiles and the implication of the variability on the structure of the clouds.

2. Observations

We used the Very Large Array (VLA) of the National Radio Astronomy Observatory (NRAO) to observe the 6 cm line of H₂CO ($J_{KaKc} = 1_{10}-1_{11}$, $\nu_0 = 4829.6594$ MHz) in absorption toward the extragalactic radio sources B0212+735 (J0217+738), 3C111 (J0418+380), BL Lac (J2202+422), and NRAO150 (J0359+509). The observations were conducted on 2009 March 2 (see Table 1)¹. The quasar J0319+415 was used as baseline/bandpass calibrator and 3C48 (J0137+331) as flux density calibrator (5.58 Jy assumed at 4.8 GHz). We measured a flux density of 13.8 Jy for J0319+415. We observed with 511 channels (channel width of 3.05 kHz, 0.19 km s⁻¹), single circular polarization and a bandwidth of 1.56 MHz (96.8 km s⁻¹), however, due to aliasing effects in the VLA-JVLA transition, only an effective bandwidth of 34 km s⁻¹ was useful. The data reduction was done in the NRAO software package AIPS, and the final spectra were exported to CLASS² for analysis. Natural weighting was used to create the images to maximize signal-to-noise. All sources were self-calibrated. Details of the observation setup and synthesized beam are given in Table 1.

In the case of 3C111, we conducted a short (10 min) observation in standard VLA C-Band continuum mode (4IF; 50 MHz per IF). J0414+343 was used as complex gain calibrator. We measured a flux density of 1.4 Jy for J0414+343. The radio continuum image of 3C111 was used as initial model for the self-calibration of the 3C111 line data.

We downloaded from the VLA archive the raw-data of previous H₂CO observations of all our sources, which have been already published by Marscher et al. (1993) and Moore & Marscher (1995). We reduced the archive data in AIPS following standard procedures. The spectra were Hanning smoothed to a final channel width of 3.05 kHz (0.19 km s⁻¹). Table 1 also lists the details of the archive data discussed in this paper.

3. Results

We detected radio continuum and H₂CO absorption toward the four sources. Table 2 lists the line parameters of the H₂CO detections obtained from single-Gaussian fits. No significant variability was detected toward B0212+735 and BL Lac (Figures 1 and 2, respectively). In the upper left panels of Figures 1 and 2, we show the radio continuum images (contours) and the peak-pixel absorption images (grey scale). In the upper right panels of Figures 1 and 2, we show the March 2009 spectra, including a fit to the six hyperfine com-

¹VLA project number AA327.

²CLASS is part of the GILDAS software package developed by IRAM.

ponents (blue dashed lines; Table 3). The lower left sequence of panels show the March 2009 spectrum (in black) and the spectra from the VLA archive obtained at previous epochs (in red). The lower right sequence of panels show the difference between the previous observations and the 2009 data. In contrast to B0212+735 and BL Lac, significant variability was detected toward NRAO 150 (Figure 3).

These three sources (B0212+735, BL Lac, NRAO 150) show compact radio emission. In contrast, 3C111 was resolved in a central compact source (Core), and two extended radio lobes to the NE and SW (see Figure 4). The H₂CO spectra and hyperfine fits of the NE and SW components are also shown in Figure 4. The low signal-to-noise toward the NE and SW regions precludes meaningful analysis of time variability, thus, only the 2009 spectra are shown. The signal-to-noise toward the 3C111 Core is as good as that of B0212+735, NRAO 150 and BL Lac, and variability is detected (Figure 5).

4. Analysis and Discussion

4.1. Reproducibility of Spectral Line Results

To check the effect of different calibration procedures, we reduced all archive observations of the sources which have been already published by Marscher et al. (1993) and Moore & Marscher (1995). We applied completely independent flagging, calibration and imaging procedures. In our analysis of the physical parameters of the clouds, the peak optical depths and linewidths are input parameters (see section 4.2), while Moore & Marscher (1995) used equivalent widths defined as $\int \tau dv$. To compare our results to those of Moore & Marscher (1995), we measured the equivalent widths of our reduction of the M94 data. Our equivalent widths agree with Moore & Marscher (1995) values within statistical uncertainties from the fit in all sources, which shows that differences in calibration procedures are not a significant source of error in determining variability. For example, in the case of the M94 observations of B0212+735, Moore & Marscher (1995) reported $\int \tau dv = 0.0893$, $V_{LSR,F=2-2} = 3.56 \text{ km s}^{-1}$, and $FWHM_{F=2-2} = 0.84 \text{ km s}^{-1}$, while we measured $\int \tau dv = 0.091 \pm 0.012$, $V_{LSR,F=2-2} = 3.57 \pm 0.01 \text{ km s}^{-1}$, and $FWHM_{F=2-2} = 0.81 \pm 0.04 \text{ km s}^{-1}$.

We detect a strong absorption line at -17.2 km s^{-1} toward NRAO 150 (see Table 3, Figure 3). This line was included in the bandpass (different IFs) of the J91 and D90 epochs, however, the line was not included in the bandpass of the M94 and D92 epochs. As clearly seen in Figure 3, the line profile of the -17.2 km s^{-1} component is perfectly well reproduced by our 2009 observations with respect to the previous epochs, showing that the variability

of the -10.5 km s^{-1} component in NRAO 150 is not an artifact. Likewise, the -2.3 km s^{-1} velocity component in 3C111 shows no variability (compare red and black spectra in Figure 5) while the main absorption feature at -1.0 km s^{-1} does.

Careful inspection of the B0212+735 and NRAO 150 spectra (Figures 1 and 3) shows that the bandpasses are not perfectly flat; specifically, the B0212+735 spectrum has a weak absorption feature at $\sim 0 \text{ km s}^{-1}$ and NRAO 150 presents weak absorption features at -14 and -4.5 km s^{-1} (highlighted with arrows). Absorption features at these velocities have been seen before in other molecular transitions. The CO, OH, and HCO^+ spectra of B0212+735 reported by Liszt & Pety (2012) show a velocity component at $\sim 0 \text{ km s}^{-1}$ in addition to the main component at $\sim 3.5 \text{ km s}^{-1}$. In the case of NRAO 150, molecular absorption features at -14 and -4.5 km s^{-1} (in addition to the components at -17.3 and -10.5 and -8.5 km s^{-1}) have been reported by Pety et al. (2008) in CO, HCO^+ , C_2H , and HNC; of all, the HNC spectrum is the most similar to the H_2CO spectrum. The same weak absorption features are seen at the other epochs (see Figure 3, left spectra). The remarkable reproducibility of these weak features demonstrates the superb stability of the VLA for long-term variability studies of spectral lines.

4.2. Physical Parameters

We used the `Molpop-CEP` code (Elitzur & Asensio Ramos 2006) to explore the physical conditions of the foreground clouds based on the observed H_2CO absorption lines. We used the H_2CO – para- H_2 collision rates of Troscompt et al. (2009b), and included He collisions using the rates by Green (1991)³. Diffuse/translucent clouds have densities between $\sim 10^2$ and $\sim 10^4 \text{ cm}^{-3}$ (e.g., van Dishoeck & Black 1988), and according to Moore & Marscher (1995) may contain even higher density clumps [$\sim 10^6 \text{ cm}^{-3}$; however see Liszt & Lucas (2000) and our discussion below]. The H_2CO abundance relative to hydrogen may be somewhere between 10^{-9} and $\sim 5 \times 10^{-8}$; for example, Zhou et al. (1990) estimated an abundance of 2×10^{-9} toward B335; Turner (1993) report an abundance of 6×10^{-9} ; Troscompt et al. (2009a) obtained an abundance of 6×10^{-8} . We ran grids of models at two kinetic temperatures (10 and 30 K), in a range of densities between 10^2 to 10^6 cm^{-3} and H_2CO abundance ratios between 10^{-9} and 5×10^{-8} , however, for the analysis, we further constrain the parameters as follows:

³Electron collisions could be an important factor in the H_2CO excitation in translucent/diffuse clouds (e.g., Turner 1993), however development of a model including electron collisions is beyond the scope of this work.

Temperature: The extinction toward the extragalactic sources discussed here is $A_V \sim 1$ mag or greater (e.g., Marscher et al. 1993; Schlegel et al. 1998; Pety et al. 2008; Schlafly & Finkbeiner 2011; Liszt & Pety 2012). Hence, the foreground clouds are in the diffuse/translucent boundary; which are expected to be hotter than ~ 10 K at their centers and as hot as ~ 50 K at their boundaries (e.g., van Dishoeck & Black 1988). Given that the H_2CO molecules are not expected at the boundaries of the clouds but at higher depths where they may be shielded from the interstellar radiation field, a temperature of ~ 30 K is assumed.

Density: observations of 6 cm H_2CO absorption profiles in a number of environments including dark nebulae, pre-protostellar cores and low mass star forming regions with absorption against the CMB (e.g., Palmer et al. 1969; Heiles 1973; Dieter 1973; Young et al. 2004; Araya et al. 2006) have resulted in excitation temperature measurements of the 6 cm K-doublet of $\lesssim 2$ K, which according to our model imply densities below $\sim 10^5 \text{ cm}^{-3}$. This is the well known result that the 6 cm H_2CO K-doublet thermalizes at densities of $\sim 10^6 \text{ cm}^{-3}$ (e.g., Troscompt et al. 2009a; Mundy et al. 1987). Thus, most of the H_2CO gas likely traces regions of densities below $\sim 10^5 \text{ cm}^{-3}$. A lower limit of the density can be inferred from our data as well: as highlighted in Figures 1 and 3 upper-right panels and discussed above, we detected some weak H_2CO absorption features. These velocity components are quite prominent in CO and HCO^+ (e.g., Pety et al. 2008), and may trace molecular gas at densities of $\sim 10^2 \text{ cm}^{-3}$ (e.g., Liszt & Lucas 2000; Pety et al. 2008). H_2CO is likely weaker because higher density conditions would be needed for stronger H_2CO absorption features (Pety et al. 2008). Thus, the H_2CO gas likely traces material at densities between $\sim 10^3$ to 10^5 cm^{-3} , i.e., higher than those traced by HCO^+ and lower than thermalization densities; we therefore assume a density of 10^4 cm^{-3} for the analysis.

Abundance: we simply assume an abundance of 5×10^{-9} , i.e., similar to the abundance reported by Turner (1993) for high-latitude cirrus clouds.

Based on these assumptions, we can calculate the H_2CO and H_2 column densities, and the thickness (ΔL) of the absorbing region (assuming a slab geometry), i.e., the depth of the cloud that would result in the observed absorption spectrum for a given density, temperature and abundance. We note that the slab thickness should be considered an effective thickness, more precisely, a lower limit of the physical path which would differ from the true thickness of the cloud depending on the number of molecular clumps and their separation along the line of sight (see Marscher et al. 1993).

In the case of the H_2CO absorption region toward the core of 3C111 (see Figure 4), we obtained the following parameters and uncertainty ranges: $\Delta L = 1.0 \times 10^4 \text{ AU}$ ($[7 \times 10^2, 5 \times 10^5] \text{ AU}$), $N(\text{H}_2) = 1.5 \times 10^{21} \text{ cm}^{-2}$ ($[1 \times 10^{20}, 5 \times 10^{22}] \text{ cm}^{-2}$), and $N(\text{H}_2\text{CO}) =$

$7.6 \times 10^{12} \text{ cm}^{-2}$ ($[7 \times 10^{12}, 5 \times 10^{13}] \text{ cm}^{-2}$), where the ranges shown in square brackets were obtained by assuming densities between 10^3 and 10^5 cm^{-3} and formaldehyde abundances with respect to hydrogen between 10^{-9} and 5×10^{-8} . We note that H_2CO column densities of $\sim 7 \times 10^{12} \text{ cm}^{-2}$ have been reported in diffuse clouds, including the ones discussed here (see Liszt et al. 2006).

Even though the value of ΔL is not well constrained within a density range of 10^3 to 10^5 cm^{-3} , we can assess how reasonable the $\Delta L = 1.0 \times 10^4 \text{ AU}$ value is. As pointed out by Moore & Marscher (1995), the extended brightness distribution of 3C111 enables a study of spatial changes of the H_2CO absorption by comparing spectral lines toward the NE, Core, and SW continuum sources. Detection of absorption along the three sight-lines shows that the overall cloud is more extended than the projected separation of the NE and SW components, i.e., $7 \times 10^4 \text{ AU}$ (0.3 pc) assuming a distance of 350 pc (Moore & Marscher 1995; obtained from a photometric/extinction analysis by Ungerechts & Thaddeus 1987)⁴. A $\Delta L = 1.0 \times 10^4 \text{ AU}$ would imply that the depth of the cloud is somewhat less than the extent of the cloud in the plane of the sky, which is consistent with having slightly different line parameters toward the different continuum sources (Table 3)⁵.

Assuming the same values of kinetic temperature (30 K), density (10^4 cm^{-3}), H_2CO abundance (5×10^{-9}), and abundance/density domains as above, we obtain a total molecular column density and slab thickness equal to $N(\text{H}_2) = 3 \times 10^{20} \text{ cm}^{-2}$ ($[3 \times 10^{19}, 5 \times 10^{21}] \text{ cm}^{-2}$) and $\Delta L = 2 \times 10^3 \text{ AU}$ ($[6 \times 10^1, 1 \times 10^5] \text{ AU}$) for B0212+735. In the case of NRAO 150 we obtain $N(\text{H}_2) = 6 \times 10^{20} \text{ cm}^{-2}$ ($[6 \times 10^{19}, 1 \times 10^{22}] \text{ cm}^{-2}$) and $\Delta L = 4 \times 10^3 \text{ AU}$ ($[2 \times 10^2, 2 \times 10^5] \text{ AU}$), while for BL Lac we obtain $N(\text{H}_2) = 2 \times 10^{20} \text{ cm}^{-2}$ ($[2 \times 10^{19}, 2 \times 10^{21}] \text{ cm}^{-2}$) and $\Delta L = 10^3 \text{ AU}$ ($[3 \times 10^1, 5 \times 10^4] \text{ AU}$).

⁴For consistency with Moore & Marscher (1995) we use the same distance they assumed for the foreground cloud, however, the possible association with the California Molecular Cloud would imply a distance of $\sim 450 \text{ pc}$ (Harvey et al. 2013).

⁵We note that velocity components at -1 km s^{-1} and 2 km s^{-1} were detected toward the Core and the NE regions, whereas only a single broad line was detected in our lower signal-to-noise spectrum of the SW 3C111 region. Thus, the significantly different H_2CO SW 3C111 profile could be caused in part due to blended lines in the low signal-to-noise spectrum.

4.3. Physical Scales Probed by the Monitoring Observations

The most important aspect to relate absorption variability to cloud structure is to be able to convert time-lapses to physical displacement of the clouds perpendicular to our sight line, i.e., the proper motion due to the combined effect of Earth’s revolution and the motion of the Solar System and the cloud around the Galaxy. Marscher et al. (1993) and Moore & Marscher (1995) estimated that the magnitude of transverse displacement for the foreground clouds toward NRAO 150, 3C111 and BL Lac is of the order of ~ 4 AU per year. Specifically, Moore & Marscher (1995) report that after approximately 3.4 years of monitoring observations, the foreground clouds toward NRAO 150 and BL Lac would have had transverse displacements of 13.9 AU and 12.4 AU, respectively. These estimates depend on the precise knowledge of the transverse velocity of the foreground clouds with respect to Earth, which has not been directly measured. Thus, we recalculated the transverse displacement of the foreground clouds including uncertainty in the cloud’s peculiar velocity around the Galaxy, in addition to the line-of-sight displacements due to Earth’s revolution, LSR reference frame correction, peculiar velocity of the Solar System and estimated Galactic circular rotation of the foreground clouds. To calculate the Galactic circular rotation, we assumed the distances reported by Moore & Marscher (1995), i.e., 700 pc (kinematic distance, Marscher et al. 1993), 350 pc (estimated from a photometric/extinction analysis by Ungerechts & Thaddeus 1987), and 330 pc (estimated from the average vertical height of Galactic molecular clouds in the solar neighborhood and the galactic latitude of the foreground cloud, Lucas & Liszt 1993) for the NRAO 150, 3C111, and BL Lac foreground clouds, respectively. We used the rotation curve of Clemens (1985) for consistency with Marscher et al. (1993). To estimate the range of possible transverse displacements, we assume a peculiar velocity of the foreground clouds of ± 10 km s⁻¹ in the three galactocentric cylindrical coordinates. In a time lapse of 748 days [the time lapse of the Marscher et al. (1993) observations], we obtain a maximum displacement of ~ 10 AU and a minimum of ~ 0 AU depending on the peculiar velocity of the clouds toward NRAO 150, 3C111 and BL Lac. This range encompasses the displacements quoted by Marscher et al. (1993), but shows that the peculiar velocity of the foreground clouds has a significant effect on the displacement, and hence, on our ability to “translate” time-lapses into transverse displacements.

The new 2009 observations reported here enable us to study variability in a time lapse of almost two-decades. From 1990 to 2009, the maximum estimated displacement is $\lesssim 100$ AU and as small as its parallax motion ($\lesssim 1$ AU; i.e., the case when the peculiar velocity of the cloud results in no proper motion) for NRAO 150, 3C111, and BL Lac. An estimate of the transverse displacement for B0212+735 is uncertain because there is no distance measurement to the foreground cloud reported in the literature, and kinematic distances (e.g., Watson et al. 2003) or statistical distances (e.g., Magnani et al. 1985) are unreliable

given the Galactic latitude and the small V_{LSR} velocity of the absorption. However, a similar displacement range is expected for the foreground cloud in B0212+735 because the magnitude of its V_{LSR} is within that of 3C111 and NRAO 150 (Table 3), and the magnitude of its galactic latitude ($|b| = 12^\circ$) is similar to that of BL Lac ($|b| = 10.4^\circ$) and 3C111 ($|b| = 8.8^\circ$).

4.4. Variability

Figures 3 and 5 bottom right panels show the difference between the 2009 spectra and the previous observations for all sources (i.e, “red” minus “black” spectra of the corresponding left panel), which will be called *residual spectra* hereafter. As mentioned above, clear variability is seen toward NRAO 150 and 3C111 Core, however the variability behavior observed toward both sources is quite different.

In the case of 3C111 Core, we found no long-term variability trend. The 2009 spectrum is the same within the noise to the September 1991 and December 1990 spectra, and only one channel from the 1994 spectrum differs by $\sim 3.5\sigma$ with respect to the 2009 spectrum. Moore & Marscher (1995) reported variability of the H_2CO line from the July 1991 and December 1992 epochs with respect to their May 1994 spectrum. We also find variability above 3σ when comparing our 2009 spectrum with the July 1991 and December 1992 data (Figure 5). Comparing the March 2009 spectrum to the December 1992 spectrum (D92–M09 residual spectrum in Figure 5), we see a line that resembles an inverse-P Cygni profile, which may be caused by a small velocity difference ($\sim 0.04 \text{ km s}^{-1}$; see Table 2) between the two different sight-lines sampled on March 2009 and December 1992. Evidence for such velocity shift was pointed out by Moore & Marscher (1995) when comparing their 1992 and 1994 spectra. The velocity difference is less than the FWHM of the line, thus, velocity gradients within the cloud could be responsible for the observed variability. We note that the M94–M09 residual spectrum shows a similar profile than the D92–M09 residual spectrum, albeit with significantly less signal to noise. We do not detect evidence for such residual line profile in the other epochs, nor toward the other sources, and at this point it is unclear why only the M92–M09 residual spectrum shows such a pronounced profile. Follow up observations of 3C111 are needed to detect more occurrences of velocity shifts and detailed analysis of synthetic spectra from computer simulations of turbulent clouds is needed to estimate the expected occurrence rate of such events.

Figure 5 also shows that the peak of the July 1991 spectrum is less deep than the March 2009 spectrum by $\Delta e^{-\tau} \sim 0.025$; Moore & Marscher (1995) also report less absorption in the July 1991 spectrum with respect to the May 1994 spectrum by $\Delta e^{-\tau} \sim 0.02$ (see their

Figure 5), however the line in our residual spectrum is narrower than that from Moore & Marscher (1995). The 3C111 residual spectra do not show evidence of hyperfine structure due to low signal-to-noise, which as mentioned in the introduction, would strengthen the case for variability.

The difference between the July 1991 and March 2009 3C111 spectra could be explained by a change in the line-of-sight overall characteristics of the foreground cloud. Recalling that the main absorption feature in 3C111 Core is consistent with $n(H_2) = 10^4 \text{ cm}^{-3}$, $T_K = 30 \text{ K}$, 5×10^{-9} H₂CO abundance, $\Delta L = 10^4 \text{ AU}$, the difference between the July 1991 and March 2009 could be caused by an $\sim 8\%$ variability in overall H₂CO abundance without changing any other parameter. Smaller abundance gradients would be needed to explain the variability if the depth (ΔL) of the H₂CO absorption region would also have changed. Significant H₂CO abundance gradients in molecular clouds are known to occur, e.g., Young et al. (2004) found clear evidence of H₂CO depletion in the interior of pre-protostellar cores.

In the case of NRAO 150 (Figure 3), our new 2009 spectrum confirms the variability trend reported by Moore & Marscher (1995), i.e., the main absorption feature has been monotonically increasing since 1990. The case of NRAO 150 shows the advantages of using H₂CO absorption as a probe for variability against point sources, in particular, the residual spectra show detection of the $F = 1 - 0$ hyperfine component and no variability of the -17.3 km s^{-1} line, which, as mentioned above, demonstrate that the residual lines are true variability and not artifacts. Figure 6 shows the variability as a function of time. The new data point shows a change in the slope of the variability, suggesting that the 1990's observations sampled a region with a greater column density/abundance gradient than the region sampled by the 2009 data.

Assuming $n(H_2) = 10^4 \text{ cm}^{-3}$, $T_K = 30 \text{ K}$, 5×10^{-9} H₂CO abundance, $\Delta L = 4 \times 10^3 \text{ AU}$ and $N(H_2CO) = 3 \times 10^{12} \text{ cm}^{-2}$, the variability observed between 1990 and 2009 can be explained by an increase of $1.3 \times 10^3 \text{ AU}$ in the effective thickness of the molecular cloud in the line of sight of the quasar (ΔL) without any change in molecular density, temperature or abundance. As mentioned above, the transverse displacement of the line of sight across the cloud between 1990 and 2009 is $\lesssim 100 \text{ AU}$. Assuming a transverse displacement of 50 AU (half the maximum expected displacement), and that the cloud has a cylindrical filamentary structure (circular cross section) with the sight line to NRAO 150 crossing the filament perpendicular to its length (Figure 7), we can calculate the radius of curvature of the circular cross section. We obtain a filament radius of $R \sim 2 \times 10^4 \text{ AU}$, and find that the line-of-sight would be crossing the filament very close to its edge (see Figure 7). We stress that the value of the radius is representative of the physical scales and not a precise measurement because of the large uncertainties involved in ΔL and transverse displacement, and the filament is

unlikely to have a perfectly circular cross-section. Nevertheless, the molecular observations by Pety et al. (2008) indeed show that the line of sight toward NRAO 150 is crossing a filamentary structure, which has projected width of $\sim 40''$ (see their Figure 4, $-12 < V < -9.5$ km s $^{-1}$ range, $5.8''$ resolution), which at a distance of 700 pc would correspond to a radius of $\sim 1.4 \times 10^4$ AU. This value is similar to the radius of $\sim 2 \times 10^4$ AU calculated above. Thus, without changing any other parameter of the overall physical conditions of the gas (e.g., temperature, abundance, density) the variability observed toward NRAO 150 could be explained by a simple geometrical effect caused by the line-of-sight crossing the edge of a molecular filament.

In order to explain the variability in H₂CO absorption profiles, Marscher et al. (1993) and Moore & Marscher (1995) argue for the presence of high density (10^6 cm $^{-3}$) molecular clumps at scales of ~ 10 AU. In contrast, here we have found that minor chemical (abundance) gradients and/or geometrical effects can account for the observed variability without the need for high density clumps. Also, high density clumps are not necessarily present in the case of foreground clouds that show no variability, such as toward B0212+735 or the -17.2 km s $^{-1}$ component toward NRAO 150. Moreover, we note that at such high densities (10^6 cm $^{-3}$) the H₂CO would be detected in emission instead of absorption against the CMB, which has never been observed in diffuse clouds.⁶ Hence, we concur with the conclusions Liszt & Lucas (2000), that presented independent arguments against explaining absorption variability as caused by AU-sized high density inclusions in interstellar clouds. In particular, Liszt & Lucas (2000) found that the high-density clump/inclusion assumption is inconsistent with the weak HCO⁺ emission in diffuse clouds. As discussed in their paper, in order to explain the weak HCO⁺ emission, a low ratio of total (high-density) clump to cloud area would be needed, but this would be inconsistent with the frequent optical depth variations observed in HCO⁺ profiles.

5. Summary

We used the Very Large Array (VLA) in 2009 to obtain a new epoch in the monitoring of 6 cm H₂CO lines from Galactic molecular clouds detected in absorption toward extragalactic radio sources. We observed Galactic absorption from diffuse/translucent molecular clouds toward B0212+735, NRAO 150, 3C111, and BL Lac. The goal of the project was to check

⁶Thermal emission of the 6 cm H₂CO line has only been seen toward the Orion BN/KL region (Zuckerman et al. 1975, see also Araya et al. 2006) and non-thermal emission has been detected only toward young massive stellar objects (e.g., Araya et al. 2008).

for variability in the absorption lines due to transverse displacement of foreground clouds with respect to our line of sight to the extragalactic continuum sources; a displacement that is caused by the combined motion of the Solar System and the foreground clouds around the Galaxy.

We detected 6 cm H_2CO absorption toward all sources. To check for the effect of different data reduction (calibration and imaging) procedures in observed spectra, we reduced the archived observations reported by Marscher et al. (1993) and Moore & Marscher (1995). Our new spectra, together with the observations reduced from the archive, demonstrate the superb stability of the VLA for long term variability studies of absorption lines. The data reported here, in particular the spectra obtained toward NRAO 150, show the advantages of using 6 cm H_2CO absorption for this type of variability studies given the detection of multiple absorption lines in the same line of sight and the presence of the $F = 1 - 0$ hyperfine component that can be used to rule out spurious variability in the main line.

We did not detect significant variability toward B0212+735 and BL Lac. Variability in the archive observations of 3C111 is seen which can be explained by relatively minor chemical (abundance), velocity and/or cloud-thickness gradients in the foreground cloud. In the case of NRAO 150, we confirm the monotonic increase in H_2CO absorption reported by Moore & Marscher (1995). We found that the monotonic variability can be explained by a filamentary (cylindrically)-shaped cloud crossing the line of sight to the quasar, i.e., the variability could be caused by simple geometrical effects without the need of high density molecular substructure (clumps or inclusions) in the medium, in agreement with Liszt & Lucas (2000). If the line of sight toward NRAO 150 is probing the edge of a foreground molecular filament as suggested by our analysis and as seen in CO maps of the region (Pety et al. 2008), then, continuing monitoring of the H_2CO absorption toward this radio source is important to further study the structure of the filament and to explore other effects such as H_2CO depletion at higher extinctions across the cloud.

The National Radio Astronomy Observatory is a facility of the National Science Foundation operated under cooperative agreement by Associated Universities, Inc. We acknowledge the anonymous referee for a careful review of the manuscript and insightful suggestions. This work has made use of the computational facilities donated by Frank Rodeffer to the Astrophysics Research Laboratory of Western Illinois University. E.D.A. acknowledges support from the Provost Travel Award and the WIU Physics Department to present some of these results at an AAS meeting. This research has made use of NASA’s Astrophysics Data System, and the NASA/IPAC Extragalactic Database (NED) which is operated by the Jet Propulsion Laboratory, California Institute of Technology, under contract with the National Aeronautics and Space Administration.

REFERENCES

- Araya, E., Hofner, P., Goss, W. M., et al. 2007, *ApJS*, 170, 152
- Araya, E. D., Hofner, P., Goss, W. M., et al. 2008, *ApJS*, 178, 330
- Araya, E., Hofner, P., Olmi, L., Kurtz, S., & Linz, H. 2006, *AJ*, 132, 1851
- Clemens, D. P. 1985, *ApJ*, 295, 422
- Dickel, H. R., Goss, W. M., & De Pree, C. G. 2001, *AJ*, 121, 391
- Dieter, N. H. 1973, *ApJ*, 183, 449
- Dieter-Conklin, N. 2009, *AJ*, 137, 3920
- Dieter-Conklin, N. 2010, *AJ*, 140, 628
- Elitzur, M., & Asensio Ramos, A. 2006, *MNRAS*, 365, 779
- Garrison, B. J., Lester, W. A., Jr., Miller, W. H., & Green, S. 1975, *ApJ*, 200, L175
- Green, S. 1991, *ApJS*, 76, 979
- Harvey, P. M., Fallscheer, C., Ginsburg, A., et al. 2013, *ApJ*, 764, 133
- Heiles, C. 1973, *ApJ*, 183, 441
- Liszt, H., & Lucas, R. 2000, *A&A*, 355, 333
- Liszt, H. S., Lucas, R., & Pety, J. 2006, *A&A*, 448, 253
- Liszt, H. S., & Pety, J. 2012, *A&A*, 541, A58
- Lucas, R., & Liszt, H. S. 1993, *A&A*, 276, L33
- Magnani, L., Blitz, L., Mundy, L. 1985, *ApJ*, 295, 402
- Mangum, J. G., Darling, J., Menten, K. M., & Henkel, C. 2008, *ApJ*, 673, 832
- Marscher, A. P., Moore, E. M. & Bania, T. M. 1993, *ApJ*, 419, L101
- Moore, E. M., & Marscher, A. P. 1995, *ApJ*, 452, 671
- Mundy, L. G., Evans, N. J., II, Snell, R. L., & Goldsmith, P. F. 1987, *ApJ*, 318, 392
- Palmer, P., Zuckerman, B., Buhl, D., & Snyder, L. E. 1969, *ApJ*, 156, L147

- Pety, J., Lucas, R., & Liszt, H. S. 2008, *A&A*, 489, 217
- Schlaflly, E. F., & Finkbeiner, D. P. 2011, *ApJ*, 737, 103
- Schlegel, D. J., Finkbeiner, D. P., & Davis, M. 1998, *ApJ*, 500, 525
- Snyder, L. E., Buhl, D., Zuckerman, B., & Palmer, P. 1969, *Phys. Rev. Lett.*, 22, 679
- Thaddeus, P. 1972, *ApJ*, 173, 317
- Townes, C. H., & Cheung, A. C. 1969, *ApJ*, 157, L103
- Troscompt, N., Faure, A., Maret, S., et al. 2009a, *A&A*, 506, 1243
- Troscompt, N., Faure, A., Wiesenfeld, L., Ceccarelli, C., & Valiron, P. 2009b, *A&A*, 493, 687
- Tucker, K. D., Tomasevich, G. R. & Thaddeus, P. 1970, *ApJ*, 161, L153
- Turner, B. E. 1993, *ApJ*, 410, 140
- Ungerechts, H., & Thaddeus, P. 1987, *ApJS*, 63, 645
- van Dishoeck, E. F., & Black, J. H. 1988, *ApJ*, 334, 771
- Watson, C., Araya, E., Sewilo, M., Churchwell, E., Hofner, P., & Kurtz, S. 2003, *ApJ*, 587, 714
- Young, K. E., Lee, J.-E., Evans, N. J., II, Goldsmith, P. F., & Doty, S. D. 2004, *ApJ*, 614, 252
- Zhou, S., Evans, N. J., II, Butner, H. M., et al. 1990, *ApJ*, 363, 168
- Zuckerman, B., Palmer, P., & Rickard, L. J. 1975, *ApJ*, 197, 571

Table 1. Observation Summary

Line of Sight	Run ⁺	R.A. (J2000) (h m s)	Decl. (J2000) (° ' ")	BW (km s ⁻¹)	Δv (km s ⁻¹)	Synthesized Beam ($\theta_{max} \times \theta_{min}$; P.A.)
B0212+735	M09	02 17 30.813	+73 49 32.62	96.8	0.19	2.7'' × 1.4'', 83°
	M94	02 17 30.819	+73 49 32.67	12.0	0.095	0.69'' × 0.44'', 41°
	D92	02 17 30.819	+73 49 32.67	12.0	0.095	0.60'' × 0.40'', 14°
NRAO 150	M09	03 59 29.747	+50 57 50.16	96.8	0.19	1.3'' × 1.1'', -16°
	M94	03 59 29.746	+50 57 50.22	12.0	0.095	0.56'' × 0.47'', 56°
	D92	03 59 29.746	+50 57 50.22	12.0	0.095	0.48'' × 0.40'', 2°
	J91	03 59 29.742	+50 57 50.13	20.0	0.095	0.52'' × 0.41'', 45°
3C111	D90	03 59 29.746	+50 57 50.22	48.3	0.19	5.5'' × 4.5'', 3°
	M09*	04 18 21.277	+38 01 35.80	96.8	0.19	2.3'' × 1.4'', -87°
	M94	04 18 21.299	+38 01 35.77	12.0	0.095	0.50'' × 0.46'', 24°
	D92	04 18 21.299	+38 01 35.77	12.0	0.095	0.45'' × 0.40'', -6°
	S91	04 18 21.298	+38 01 35.72	12.0	0.095	0.52'' × 0.46'', 70°
	J91	04 18 21.298	+38 01 35.72	12.0	0.095	0.48'' × 0.44'', -5°
BL Lac	D90	04 18 22.915	+38 01 43.27	48.3	0.19	5.5'' × 4.7'', -9°
	M09	22 02 43.291	+42 16 39.98	96.8	0.19	2.4'' × 1.7'', 63°
	M94	22 02 43.279	+42 16 40.05	12.0	0.095	0.53'' × 0.43'', -10°
	D92	22 02 43.279	+42 16 40.05	12.0	0.095	0.49'' × 0.42'', -55°
	S91	22 02 43.288	+42 16 39.89	12.0	0.095	0.49'' × 0.42'', 7°
	J91	22 02 43.288	+42 16 39.89	12.0	0.095	0.47'' × 0.40'', -6°
D90	22 02 43.279	+42 16 40.05	48.3	0.19	5.2'' × 4.8'', 34°	

Note. — The right ascension and declination of the phase tracking center are given (coordinates were precessed to J2000 equinox), as well as the bandwidth and initial channel width (all spectra were smoothed to a channel width of 0.19 km s⁻¹ for the analysis). Note that in the case of the 2009 observations, only ~ 35% of the bandwidth could be used due to aliasing. (+) The different runs correspond to 02 March 2009 (M09), 01 May 1994 (M94), 27 December 1992 (D92), 13 July 1991 (J91), 10 December 1990 (D90). The VLA project number of the 2009 observations is AA327, all other runs correspond to observations published by Moore & Marscher (1995; VLA archive project numbers AM309, AM331, AM376, AM440). (*) On the M09 run, we observed 3C111 also in continuum mode, which resulted in a synthesized beam = 3.2'' × 1.4'', P.A. = -70°.

Table 2. Line Parameters

Line of Sight	Run	$e^{-\tau}$	$\text{rms}_{e^{-\tau}}$	V_{LSR} (km s^{-1})	$FWHM$ (km s^{-1})
B0212+735	M09	0.928	0.002	3.39 (0.01)	1.06 (0.03)
	M94	0.932	0.003	3.42 (0.01)	1.11 (0.04)
	D92	0.937	0.004	3.37 (0.04)	1.08 (0.09)
NRAO 150	M09 ¹	0.810	0.002	−10.57 (0.02)	0.70 (0.04)
	M94	0.840	0.003	−10.54 (0.01)	0.69 (0.02)
	D92	0.852	0.003	−10.53 (0.01)	0.73 (0.02)
	J91	0.860	0.003	−10.52 (0.02)	0.69 (0.04)
	D90	0.870	0.005	−10.53 (0.02)	0.76 (0.04)
	M09	0.942	0.002	−17.30 (0.02)	0.76 (0.05)
	J91	0.934	0.003	−17.30 (0.02)	0.69 (0.05)
	D90	0.943	0.005	−17.3 (0.1)	0.8 (0.3)
	M09	0.984	0.002	−8.6 (0.1)	1.1 (0.2)
	M94	0.984	0.003	−8.6 (0.1)	1.0 (0.2)
	D92	0.986	0.003	−8.4 (0.2)	0.7 (0.2)
	J91	0.987	0.003	−8.4 (0.1)	0.7 (0.2)
3C111-CORE	D90	0.989	0.005	−8.4 (0.1)	0.4 (0.3)
	M09	0.677	0.002	−1.01 (0.01)	0.90 (0.01)
	M94	0.677	0.002	−1.0 (0.2)	1.0 (0.2)
	D92	0.685	0.003	−0.97 (0.05)	0.95 (0.2)
	S91	0.684	0.007	−1.0 (0.2)	1.0 (0.2)
	J91	0.695	0.005	−1.01 (0.05)	0.94 (0.03)
	D90	0.675	0.005	−1.0 (0.1)	0.90 (0.06)
	M09	0.960	0.002	−2.29 (0.07)	1.8 (0.1)
	M94	0.958	0.002	−2.6 (0.2)	1.3 (0.2)
	D92	0.960	0.003	−2.4 (0.1)	1.6 (0.1)
	S91	0.970	0.007	−2.7 (0.2)	1.3 (0.2)
	J91	0.960	0.005	−2.4 (0.1)	1.6 (0.3)
	D90	0.956	0.005	−2.4 (0.1)	1.6 (0.2)
	3C111-NE	M09	0.70	0.01	−1.15 (0.02)
M94		0.71	0.03	−1.1 (0.2)	0.8 (0.2)
D92		0.68	0.05	−1.19 (0.04)	0.6 (0.2)
S91		0.56	0.09	−1.13 (0.07)	1.0 (0.2)
J91		0.60	0.07	−1.10 (0.05)	0.7 (0.1)
D90		0.69	0.01	−1.1 (0.2)	0.9 (0.2)
M09		0.93	0.01	−2.46 (0.05)	1.3 (0.2)
M94		0.94	0.03	−2.3 (0.2)	1.5 (0.2)
D90		0.91	0.01	−2.5 (0.2)	1.2 (0.2)
3C111-SW	M09	0.68	0.05	−1.67 (0.07)	1.4 (0.2)
	M94	...	0.4
	D92	...	0.3
	S91	...	0.6
	J91	...	0.4
	D90	0.83	0.06	−1.7 (0.1)	2.0 (0.3)
BL Lac ²	M09	0.957	0.002	−1.57 (0.03)	0.95 (0.07)
	M94	0.958	0.002	−1.62 (0.03)	0.93 (0.05)

Table 2—Continued

Line of Sight	Run	$e^{-\tau}$	$\text{rms}_{e^{-\tau}}$	V_{LSR} (km s^{-1})	$FWHM$ (km s^{-1})
	D92	0.961	0.002	−1.66 (0.04)	0.88 (0.07)
	S91	0.958	0.002	−1.56 (0.02)	0.88 (0.04)
	J91	0.959	0.002	−1.55 (0.02)	1.01 (0.05)
	D90	0.957	0.004	−1.62 (0.07)	1.0 (0.1)
	M09	0.984	0.002	−0.41 (0.06)	1.11 (0.14)
	M94	0.984	0.002	−0.46 (0.07)	1.06 (0.18)
	D92	0.984	0.002	−0.5 (0.1)	1.3 (0.3)
	S91	0.983	0.002	−0.52 (0.04)	0.7 (0.1)
	J91	0.986	0.002	−0.37 (0.05)	0.8 (0.1)
	D90	0.987	0.004	−0.5 (0.2)	1.0 (0.4)

Note. — Unless indicated otherwise, the line parameters were obtained by fitting the main group of five hyperfine components with a single Gaussian profile; the $F = 1 - 0$ hyperfine component was excluded from the fit. ⁽¹⁾ Gaussian fit underestimates optical depth. The peak $e^{-\tau}$ and channel velocity are 0.790 and -10.48 km s^{-1} ; see Table 3 for fit including hyperfine structure. ⁽²⁾ Complex absorption profile fitted with two Gaussians. The weaker Gaussian profile overlaps with the $F = 1 - 0$ hyperfine component of the strong line.

Table 3. Hyperfine Fit of 2009 Spectra

Line of Sight	τ_ν (F=2-2)	V_{LSR} (km s ⁻¹)	$FWHM$ (km s ⁻¹)
B0212+735	0.044 (0.001)	3.54 (0.01)	0.82 (0.03)
NRAO 150	0.17 (0.03)	-10.47 (0.03)	0.40 (0.07)
	0.05 (0.02)	-17.2 (0.1)	0.4 (0.3)
3C111-CORE ¹	0.243 (0.004)	-0.87 (0.01)	0.65 (0.01)
3C111-NE	0.24 (0.01)	-1.01 (0.01)	0.56 (0.02)
3C111-SW	0.20 (0.02)	-1.51 (0.05)	1.1 (0.1)
BL Lac ²	0.023 (0.009)	-1.54 (0.10)	0.57 (0.25)
	0.010 (0.005)	-0.80 (0.23)	0.96 (0.55)

Note. — Line parameters obtained by fitting the six hyperfine components of the H₂CO line. Resulting fits are shown in Figures 1 to 5 (blue dashed curves). LTE line intensities were assumed (Tucker et al. 1970). The optical depth corresponds to the $F = 2 - 2$ transition. 1σ errors from the fit are shown in parenthesis. ⁽¹⁾ A second velocity component overlaps with the main absorption line. The line parameters of the overlapping line are $V_{LSR} = -2.29$ km s⁻¹, $FWHM = 1.8$ km s⁻¹, $\tau = 0.0356$. ⁽²⁾ A reliable hyperfine fitting of the line could not be obtained due to overlapping velocity components. We report the hyperfine line parameters assuming two velocity components. However, a third velocity component is still needed to account for the absorption at 0.3 km s⁻¹ (Figure 2, upper right panel).

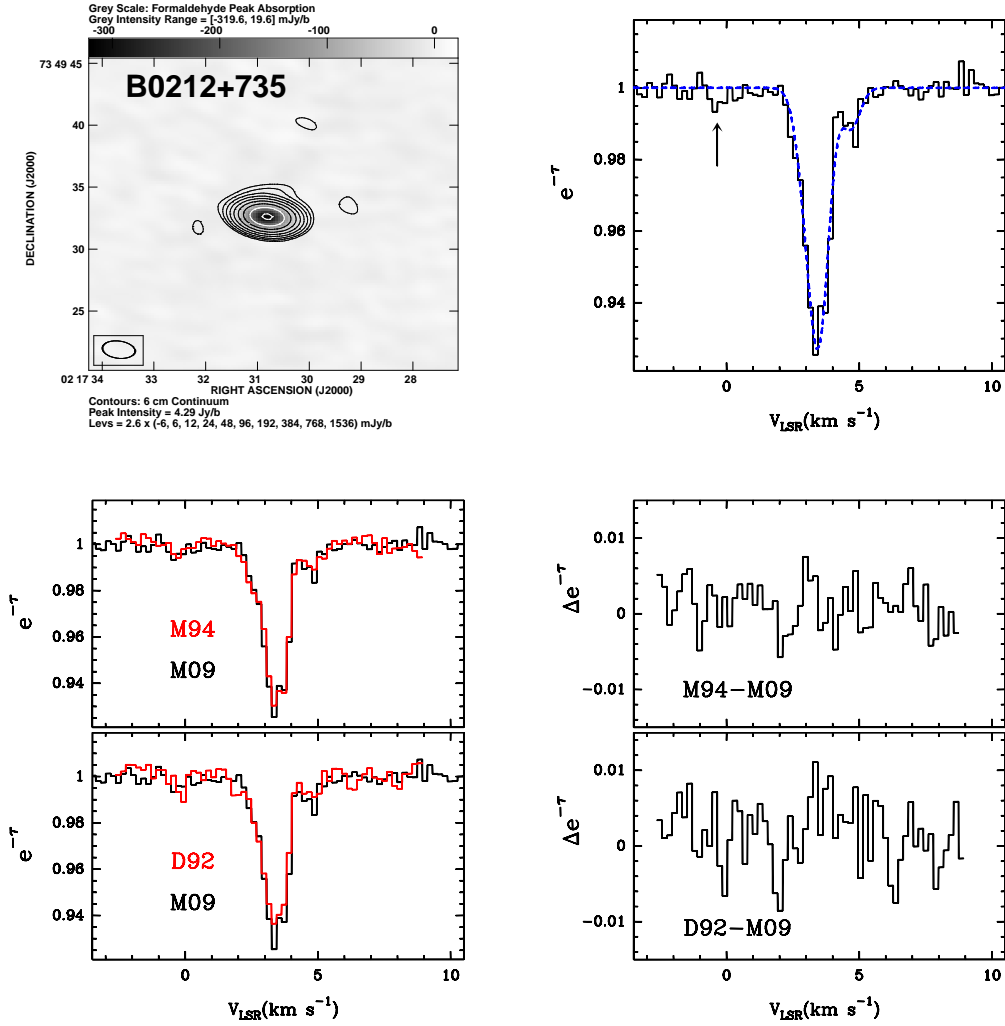


Fig. 1.— *Upper left panel:* Radio continuum image of the extragalactic radio source B0212+735 is shown in contours; the gray scale shows the distribution of the peak H₂CO absorption toward the quasar (minimum value of the H₂CO spectrum in each pixel). *Upper right panel:* Spectrum obtained in the March 2009 run of this project. The blue dashed line is the fit to the six hyperfine components of the transition (Table 3). The arrow highlights a weak absorption feature. *Middle and bottom left panels* show the M09 spectra (black) and the spectra from the other epochs (red); the difference between the red and black spectra are presented in the *middle and bottom right panels*.

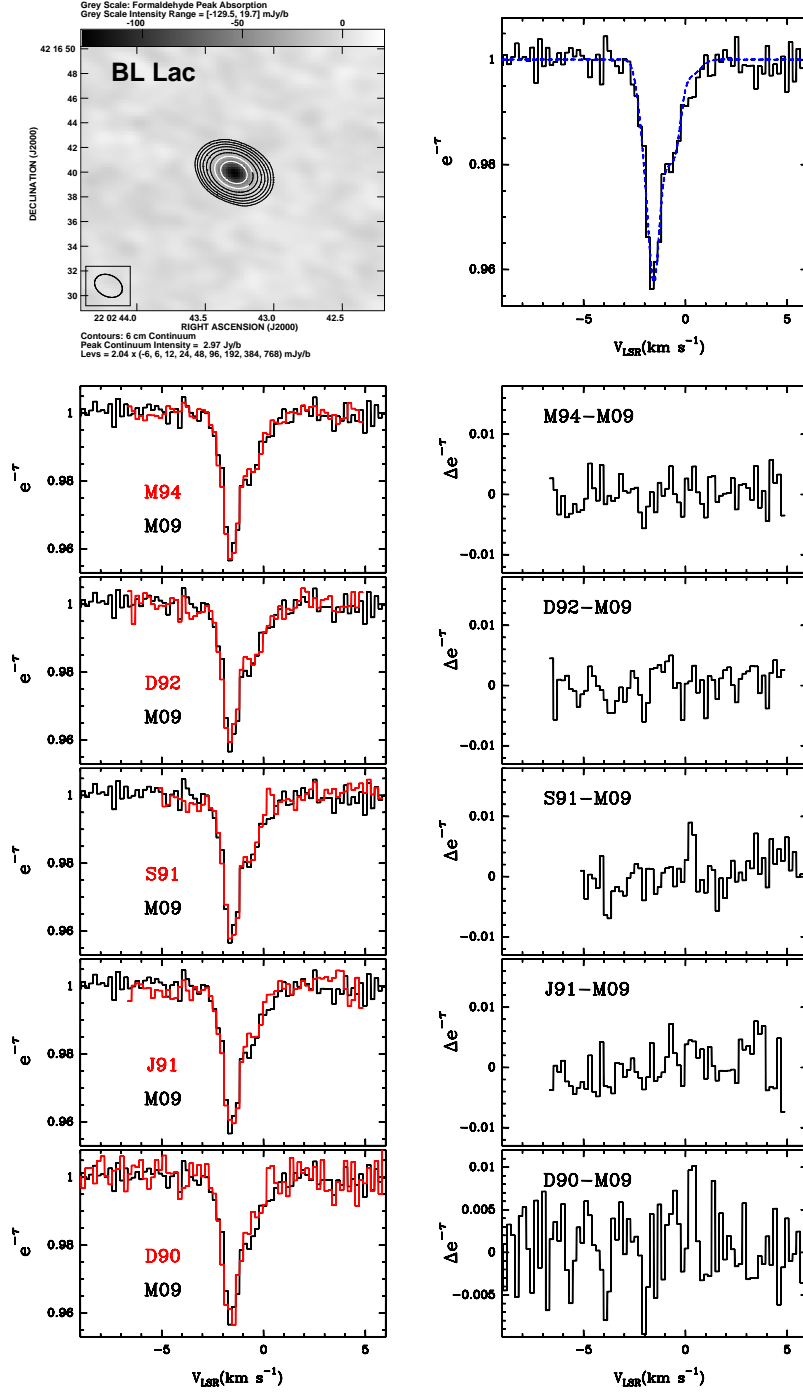


Fig. 2.— Same as Figure 1 for BL Lac. The blue dashed line shown in the upper right panel is the hyperfine line fit of two overlapping velocity components (see Table 3). A third velocity component ($e^{-\tau} \approx 0.993$) is needed to explain the absorption at ~ 0.3 km s⁻¹.

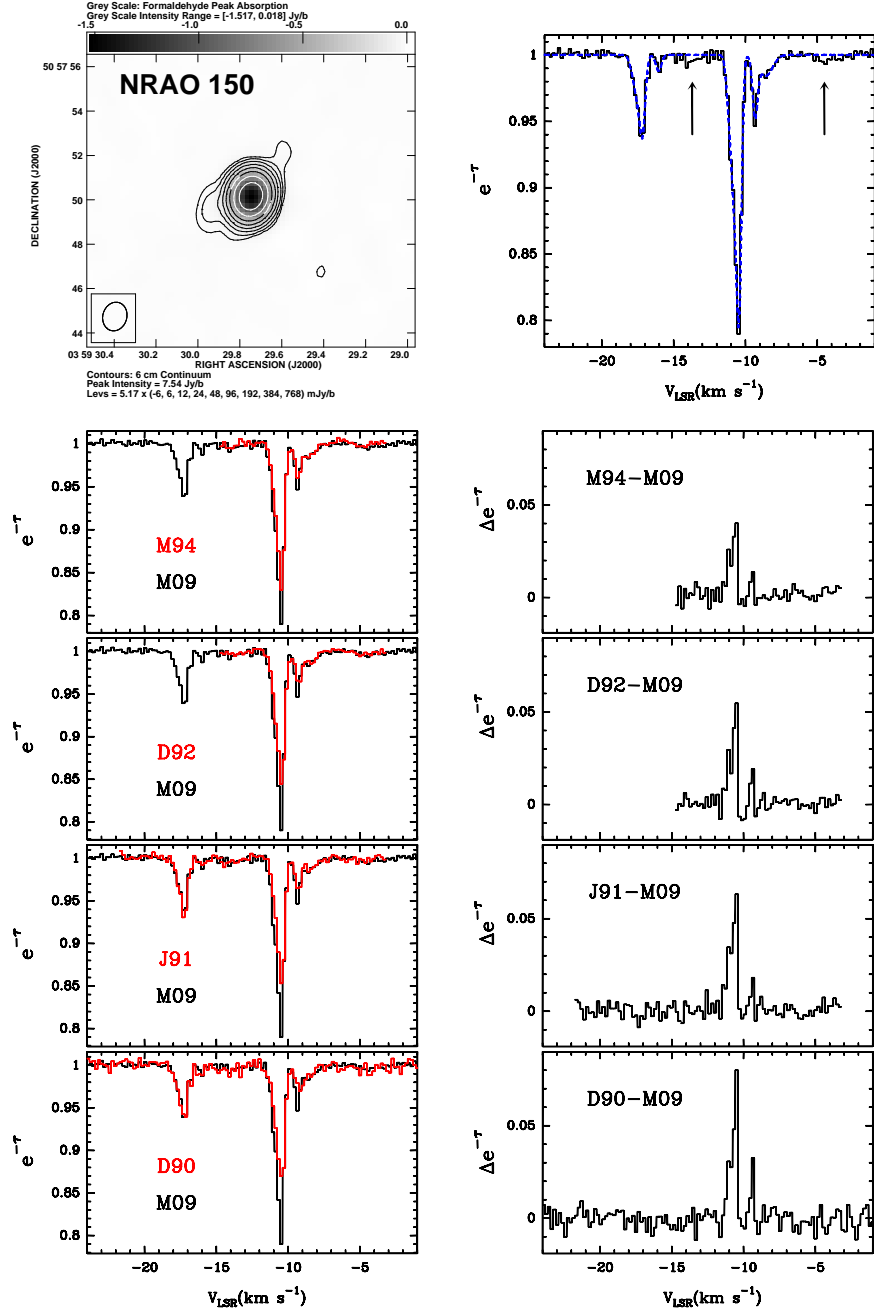


Fig. 3.— Same as Figure 1 for NRAO 150. The blue dashed line is the fit to the six hyperfine components of the transition (Table 3), however the (broad and weak) line at -8.6 km s^{-1} is not part of the hyperfine structure of the main absorption line. The line parameters of the -8.6 km s^{-1} line are given in Table 2. The narrow line at $\sim -9 \text{ km s}^{-1}$ is the $F = 1 - 0$ hyperfine component of the main line. The arrows highlight weak absorption features.

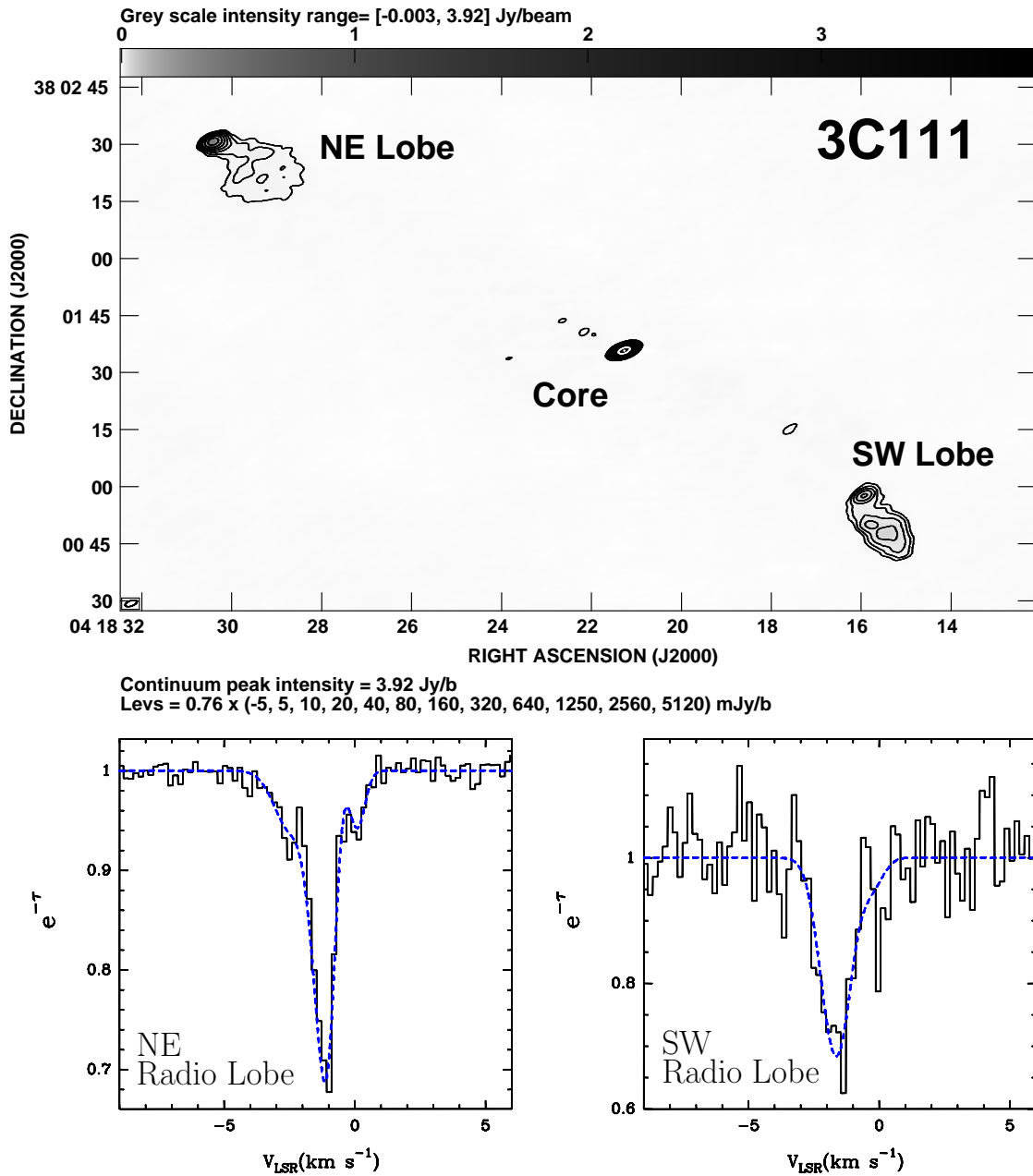


Fig. 4.— *Upper Panel:* Radio continuum image of 3C111. This image was obtained from the continuum set up observations and was used as initial model for self-calibration of the line data. *Lower Panels:* Spectra obtained in the March 2009 run toward the NE and SW radio lobes of 3C111. As in Figure 1, the blue dashed line is the fit to the six hyperfine components of the transition with the exception of the overlapping -2.46 km s^{-1} velocity component (NE 3C111 spectrum) whose parameters are reported in Table 2.

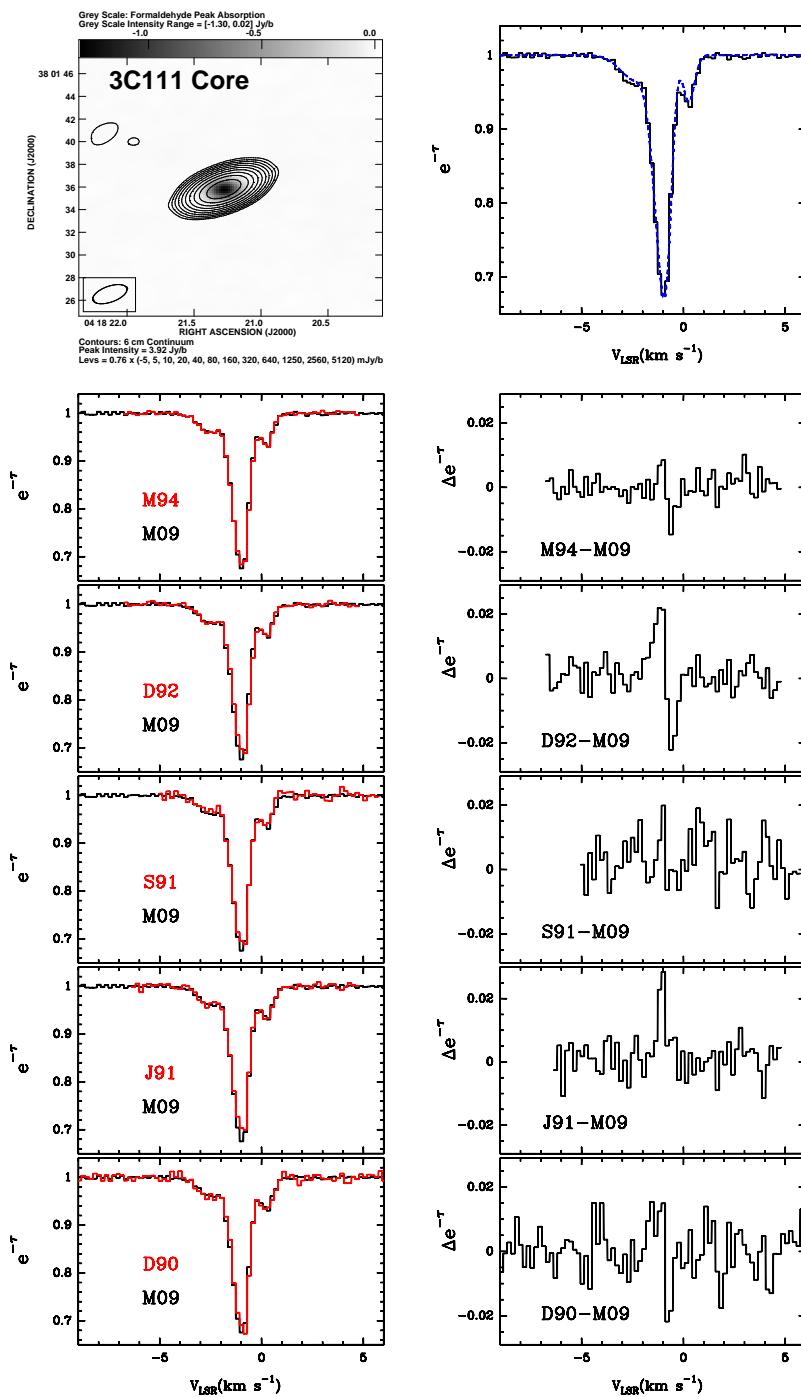


Fig. 5.— Same as Figure 1 for the 3C111 Core. Continuum is from Figure 4. A second velocity component at $\sim -2.3 \text{ km s}^{-1}$ overlaps with the main absorption line (see Table 2). Note the “inverse-P Cygni” profile of the D92-M09 residual spectrum which may be caused by a slight velocity difference between the D92 and M09 peaks (see Table 2 and Section 4.4).

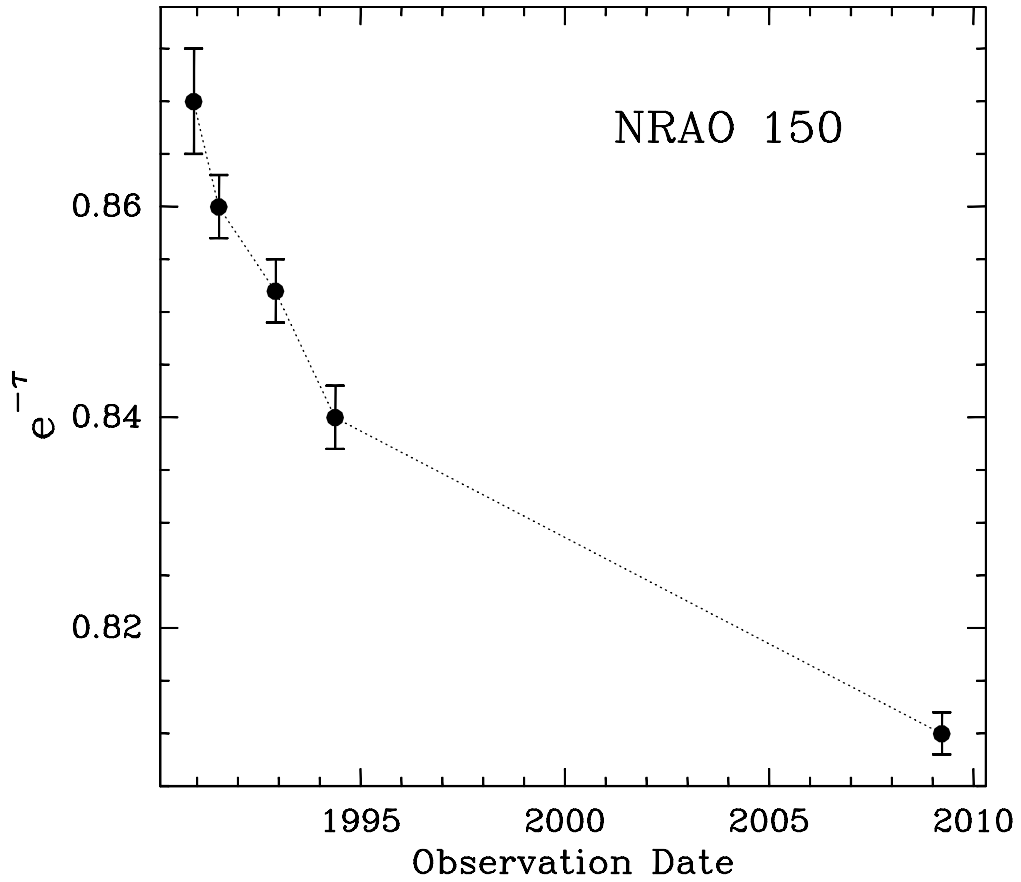
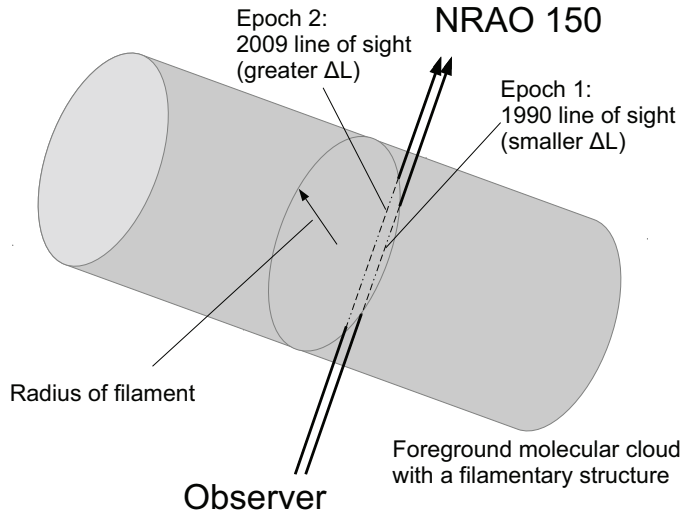


Fig. 6.— Variability of the peak H_2CO absorption line in NRAO 150 as a function of time. Our results confirm a monotonic increase in absorption, which suggests that the physical scale of the substructure sampled by the data is greater than the transverse displacement over the time period.

Side View of Molecular Cloud:



Cross-section View of Molecular Cloud:

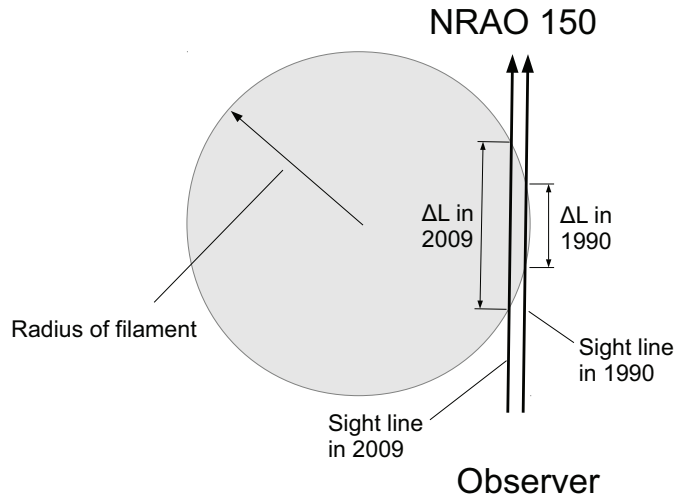


Fig. 7.— Scheme of the foreground molecular cloud geometry used to explain the variability of the H_2CO absorption profile toward NRAO 150. We assume that the transverse displacement of the line of sight toward the quasar is parallel to the cross section of the filament and moving inwards, i.e., the absorption has been increasing as a function of time, thus the line of sight path across the filament (ΔL) has been increasing since 1990.